Princeton Plasma Physics Laboratory

PPPL- 4429

PPPL- 4429

Geometry Dependence of Stellarator Turbulence

H.E. Mynick, P. Xanthopoulos and A.H. Boozer

August, 2009

Prepared for the U.S. Department of Energy under Contract DE-AC02-09CH11466.

Princeton Plasma Physics Laboratory
Report Disclaimers

Full Legal Disclaimer

Trademark Disclaimer

PPPL Report Availability

Princeton Plasma Physics Laboratory:

http://www.pppl.gov/techreports.cfm

Office of Scientific and Technical Information (OSTI):

http://www.osti.gov/bridge

Related Links:

U.S. Department of Energy

Office of Scientific and Technical Information

Fusion Links

Geometry dependence of stellarator turbulence

H.E. Mynick[a], P. Xanthopoulos[b] and A.H. Boozer[c]
[a]Plasma Physics Laboratory, Princeton University
[b]Max-Planck-Institut für Plasmaphysik, Teilinstitut Greifswald
[c]Dept. of Applied Physics & Mathematics, Columbia University

Using the nonlinear gyrokinetic code package GENE/GIST, we study the turbulent transport in a broad family of stellarator designs, to understand the geometry-dependence of the microturbulence. By using a set of flux tubes on a given flux surface, we construct a picture of the 2D structure of the microturbulence over that surface, and relate this to relevant geometric quantities, such as the curvature, local shear, and effective potential in the Schrödinger-like equation governing linear drift modes.

PACS #s: 52.55.Hc, 52.65.Tt, 52.35.Ra

The concept of "transport–optimized stellarators" (for an overview see *e.g.* Ref. 1) aims at mitigating the neoclassical (nc) losses to the point where anomalous transport becomes dominant over most of the plasma column. Attention is now turning to understanding the effects of 3D geometry on microturbulence,[2–7] aided by nonlinear gyrokinetic codes valid for 3D. Supported by the scant, albeit promising, existing findings in this area, we attempt to identify key geometrical factors which contribute to the development and, subsequently, control of turbulent transport levels.

In this Letter, we employ the GENE/GIST code package[8,9] and systematically apply its unique capability of determining turbulence properties for a 3D VMEC equilibrium[10] to a wide representative family of optimized stellarator designs (plus one reference axisymmetric system), to understand the geometry dependence of ion-temperature-gradient (ITG) turbulence.

Existing 3D nonlinear gk codes are "flux tube" codes,[11] yielding a picture of the turbulence along a particular field line, a 1D structure. To better relate such results to the full geometry, we follow a novel procedure, in order to construct the 2D structure of the turbulence over a flux-surface by combining results for a set of such field lines on that flux surface, and relate this structure to relevant geometric quantities, including the curvature, local shear, and effective potential $V_{ef}(z)$ in the Schrödinger-like equation governing linear drift modes.

The global volume of a torus is conveniently parametrized by flux coordinates $\mathbf{x} = (\psi, \theta, \zeta)$, with $2\pi\psi$ the toroidal flux within a flux surface, and θ and ζ the poloidal and toroidal azimuths, chosen so that the magnetic field may be written $\mathbf{B} = \nabla\alpha \times \nabla\psi_p$, with $2\pi\psi_p(\psi)$ the poloidal flux, $\alpha \equiv \zeta - q\theta$, and $q(\psi) \equiv \iota^{-1}$ the tokamak safety factor. In its local mode of operation, GENE simulates plasma turbulence in a field-line following coordinate system (x, y, z) within a flux tube surrounding a specified

field line, with $z = \theta$ the coordinate along a field line, $x \equiv r - r_0$, with $r(\psi) \equiv (2\psi/B_a)^{1/2}$ a minor radial variable with units of length, r_0 the value of r on the chosen flux surface, B_a a normalizing magnetic field strength, and $y \equiv -r_0\iota_0\alpha$ the in-surface Clebsch coordinate with units of length, satisfying $\mathbf{B} = B_a\nabla x \times \nabla y$. z runs for 1 full poloidal transit, and periodic boundary conditions are imposed in all 3 directions. The simulations discussed here all compute collisionless electrostatic turbulence, assuming adiabatic electrons, with parameters $a/L_n \equiv -a\partial_r n/n = 0, a/L_{Ti} \equiv -a\partial_r T_i/T_i = 3, r_0/a \simeq 0.7, \tau \equiv T_e/T_i = 1, \rho_s/L_y = .05/2\pi$, and $L_x = L_y$, with $L_{x,y}$ the box size in the x and y directions, a the value of r at the edge, $\rho_s \equiv c_s/\Omega_i$, $c_s \equiv (T_e/M_i)^{1/2}$ the sound speed, and Ω_i the ion gyrofrequency. $N_x \times N_y \times N_z = 64 \times 96 \times (96$ or $128)$ grid points were employed in the x, y, and z directions, and $N_{v_\parallel} \times N_\mu = 32 \times 8$ points in velocity space.

We study a family of configurations including a representative from each of the 3 principal approaches to nc transport optimization[1], NCSX[12], a 3 field-period ($N = 3$) quasi-axisymmetric (QA) design, HSX[13], an $N = 4$ quasi-helically-symmetric (QH) design, and W7X[14], an $N = 5$ quasi-isodynamic/quasi-omnigenous (QI/QO) design. We also simulate NCSX_sym, a fully axisymmetric (2D) equilibrium obtained from the NCSX geometry by dropping all the nonaxisymmetric Fourier components.

We construct a 2D picture of the time-averaged RMS turbulent potential amplitude $\langle\phi\rangle(\theta, \zeta|r_0)$ over the flux surface at $r = r_0$ from a set of M flux-tube GENE simulations. The simulations for tubes $j = 0, 1, .., M - 1$ are evenly spaced over a half field-period, $N\alpha_0 = 0, \pi/(M-1), .., \pi$. Each simulation produces the turbulent amplitude $\langle\phi\rangle(z|r_0, N\alpha_0)$. The value of $\langle\phi\rangle$ in the other half field-period (tubes labeled $j = -1, .., -(M-1)$) is obtained from the tubes in the simulated half-period via stellarator symmetry, $\langle\phi\rangle(-\theta, -\zeta|r_0) = \langle\phi\rangle(\theta, \zeta|r_0)$, or $\langle\phi\rangle(-z|r_0, -N\alpha_0) = \langle\phi\rangle(z|r_0, N\alpha_0)$.

The 2D strip for a single field period is then replicated N times to cover a complete flux surface. The construction for any other relevant physical quantity is essentially the same.

We begin in Figs. 1-3 by comparing $\langle\phi\rangle$ and the radial curvature component $\mathcal{K}_2 = \boldsymbol{\kappa}\cdot\mathbf{e}_x$ whose negative part denotes the "bad curvature"[16] ($\mathbf{e}_x$ is the covariant basis vector) for NCSX with that in its axisymmetrized counterpart NCSX_sym. In Fig. 1a is shown a 1D plot of $\langle\phi\rangle(z|r_0, N\alpha_0)$ for $M = 3$ flux tubes for NCSX, for $N\alpha_0 = 0$ (blue), $\pi/2$ (green), and π (red), along with a single flux tube (dashed blue) for NCSX_sym (all tubes are equivalent in a 2D torus). Fig. 2a shows the 2D plot $\langle\phi\rangle(\theta,\zeta)$ composed from these for NCSX_sym, and Fig. 3a for NCSX, with red being large values, blue low values. Figs. 1b, 2b, and 3b show the corresponding plots for $\mathcal{K}_2$. (The not quite perfect axisymmetry in Figs. 2 and the larger triangular regions near the top and bottom boundaries in Figs. 3 are artifacts of the MATLAB Delaunay triangulation routine used to combine the values from the separate flux tubes.)

For NCSX_sym, as expected, one sees that $\langle\phi\rangle$ balloons toward the outboard side ($\theta = 0$), where $\mathcal{K}_2$ is worst (most negative). As one might also expect, $\langle\phi\rangle$ and $\mathcal{K}_2$ for NCSX resemble those for NCSX_sym, but modulated by the deviations of the QA from true axisymmetry.

Shown in Figs. 4 are the 1D plots $\langle\phi\rangle$ and $\mathcal{K}_2$ for W7X, whose toroidal amplitude ϵ_t is comparable to its helical amplitude ϵ_h, characteristic of QO/QI systems. While B and $\mathcal{K}_2$ have a variation on the more rapid helical scale length L_h, the helical wells these produce in the mode equation's effective potential V_{ef} are insufficient to localize an ITG mode, leaving the longer, toroidal well to provide the dominant localization.

A similar statement holds for HSX, whose magnetic field strength $B(\mathbf{x})$ is helically symmetric to better than one part in 400, ($\epsilon_t \ll \epsilon_h$). Here, while one might expect the

toroidal ballooning evident in NCSX and NCSX_sym to be replaced by an analogous ballooning within a helical ripple period, as for W7X, L_h is too narrow to localize $\langle\phi\rangle$, as seen in Figs. 5, and as a result the turbulence in each tube still balloons toward $\theta = 0$, though not as much as for a tokamak or QA system. This surprising finding is experimentally supported by HSX probe measurements.[17]

For each of these configurations, the region of maximum $\langle\phi\rangle$ occurs where $\mathcal{K}_2$ is most negative, which is around $(\theta, N\alpha_0) \simeq (0, 0)$, *i.e.*, on the outboard side around the device "corners". The variation of the resultant heat flux $Q_i(\theta|N\alpha_0)$ along a field line qualitatively follows the variation of $\langle\phi\rangle$. As might be expected, the tube-averaged flux $\bar{Q}_i(N\alpha_0) = -n_0\bar{\chi}_i\langle\nabla T_{i0}\cdot\nabla x\rangle$ or anomalous diffusivity $\bar{\chi}_i$ varies little ($\bar{\chi}_{max}/\bar{\chi}_{min} \simeq 1.1$) for NCSX, where different flux tubes are physically similar, but varies widely ($\bar{\chi}_{max}/\bar{\chi}_{min} \simeq 3.2$) for W7X, where different tubes have quite different profiles of B and $\mathcal{K}_2$.

It has been observed[3] that $\langle\phi\rangle(\theta)$ for ITG turbulence resembles the structure of the linear modes. One may obtain an equation for the linear modes $\phi(\theta)$ from the quasineutrality condition $0 = g_e/\tau + g_i$, with response function g_s equal to $k^2\lambda_s^2$ times the linear susceptibility, yielding

$$0 = g_e/\tau + 1 - \left\langle J_0^2 \frac{\omega - \omega_{*i}^f}{\omega - k_\parallel v_\parallel - \omega_D} \right\rangle_v \simeq C(\omega) + D(\omega)(qRk_\parallel)^2, \qquad (1)$$

cubic in mode frequency ω, with velocity-space average $\langle..\rangle$, $\omega_*^f \equiv \omega_*[1 + \eta(u^2 - 3)/2]$, $u \equiv v/v_T$, thermal velocity v_T, diamagnetic and drift frequencies $\omega_* \equiv -ck_\theta\kappa_n T/(eB)$ and $\omega_D \equiv \mathbf{v}_D\cdot\mathbf{k} = \omega_d(u_\perp^2/2 + u_\parallel^2)$, $\omega_d \equiv cT_i/(e_iB^3)\mathbf{B}\times\nabla B\cdot\mathbf{k}_\perp$, $C(\omega) \equiv (c_0 + \omega^{-1}c_1 + \omega^{-2}c_2)$, $D(\omega) \equiv (\omega^{-2}d_2 + \omega^{-3}d_3)$, and coefficients c_{0-2}, d_{2-3} collecting terms in powers of ω and $k_\parallel$, *e.g.*, $c_0 \equiv g_e/\tau + 1 - I_0(b_i)e^{-b_i}$. For adiabatic electrons, $g_e = 1$.

The shape of $V_{ef} \equiv C(\omega)/D(\omega)$, shown in Fig. 6 for a single tube ($j = 2$) for each of the 4 geometries, is dominated by that of $\mathcal{K}_2$, coming from the drift term ($\propto \omega_D/\omega$) from (1). Using the replacement $ik_\parallel \rightarrow \nabla_\parallel = (B\mathcal{J})^{-1}\partial_\theta$ in (1), with Jacobian $\mathcal{J} \equiv 1/\nabla\alpha \times \nabla\psi_p \cdot \nabla\theta \equiv 1/B^\theta$, a Schrödinger-like mode equation is obtained for ϕ along a field line, $0 = [V_{ef} - (qRB^\theta/B)\partial_\theta(qRB^\theta/B)\partial_\theta)]\phi(\theta)$, in which curvature enters through V_{ef}.

The local shear $s_l = \partial_\theta(g^{xy}/g^{xx})$ (with g^{ij} the components of the metric tensor) enters Eq.(1) through locally modifying both $k_\parallel(\theta)$, and $k_\perp^2(\theta)$ through radial wavenumber $k_x(\theta)$. In Fig. 7 are compared s_l in NCSX and NCSX_sym. As for other stellarators, the much stronger shaping for NCSX makes $|s_l|$ substantially larger and more structured than for a 2D system like NCSX_sym. One might expect spikes in s_l to bound modes more than would occur just through the action of V_{ef}, since s_l causes $k_\parallel$ or k_x to locally appreciably deviate from 0, enhancing Landau damping, as well as reducing the mode radial extent, similar to the function performed nonlinearly by zonal flows. Evidence for this may be seen in comparing the spikes in s_l in Fig. 7 with the restrictions and dimples in $\langle\phi\rangle$ for NCSX in Fig. 1a. Further support is found by creating an artificial configuration, NCSX_s, obtained from NCSX by artificially doubling s_l by doubling g^{xy}, adjusting g^{yy} to preserve the field alignment constraint, and consistently modifying $\mathcal{K}_2$, which implicitly contains g^{xy}. $\langle\phi\rangle(\theta)$ in NCSX_s resembles that of NCSX, but substantially more localized, restricted by the increased peaks in $s_l(\theta)$, with $Q_i(\theta)$ correspondingly narrowed and reduced.

Summarizing, we have examined the structure of microturbulence in a broad family of transport-optimized toroidal systems using the gk code GENE. Visualizing this, and its relation to important geometric quantities, is facilitated by the construction of a 2D picture of these over a flux surface from the 1D information a flux-tube code provides.

Two such geometric quantities, $\mathcal{K}_2$ and s_l, are seen to be important for ITG turbulence in determining the parallel form of $\langle\phi\rangle$, both from the simulation results, and because both are operative in the linear mode equation, whose solutions ϕ have been observed to resemble the averaged nonlinear amplitude $\langle\phi\rangle$. For each stellarator, $\langle\phi\rangle$ is seen to peak toward the outboard side near the device corners (where $\mathcal{K}_2$ is worst), manifesting a toroidal ballooning structure, which is modulated by the helical ripples, but not enough to localize modes within them, even for HSX. Further improvements to the present results are planned, *e.g.*, incorporating the effect of an ambipolar electric field, and in taking adiabatic electrons, which removes the trapped electron drive, which can change mode characteristics.[16] A relatively simple relationship between $\langle\phi\rangle$ and identifiable geometric quantities like $\mathcal{K}_2$ and s_l, which can be quickly computed, suggests an optimization may be done with an objective function involving those quantities, to obtain a geometry which seeks to minimize the turbulent transport.

Acknowledgment

The authors are grateful to F. Jenko, F. Merz, J. Talmadge, and E. Valeo for valuable discussions. This work supported by U.S.Department of Energy Contract No.DE-AC02-09CH11466.

[1] H.E. Mynick, *Phys. Plasmas* **13**, 058102 (2006).

[2] T.-H Watanabe, H. Sugama, S. Ferrando-Margalet, *Phys. Rev. Letters*, **100** 195002 (2008).

[3] P. Xanthopoulos, F.Merz, T.Goerler, and F. Jenko, *Phys. Rev. Letters* **99**, 035002 (2007).

[4] H. Sugama, T.-H. Watanabe, *Phys. Plasmas* **16**, 056101 (2009).

[5] W. Guttenfelder, J. Lore, D.T. Anderson, F.S.B. Anderson, J.M.Canik, W. Dorland, K.M.Likin, J.N.Talmadge, *Phys. Rev. Letters* **101**, 215002 (2008).

[6] I. Calvo, B.A. Carreras, L. Garcia, *et al.*, *Plasma Phys. Controlled Fusion* **51**, 065007 (2009).

[7] S. Marsen, M. Otte, F. Wagner, *Contrib. Plasma Phys.* **48**, 467 (2008).

[8] F. Jenko, W. Dorland, M. Kotschenreuther, B.N. Rogers, *Phys. Plasmas* **7**, 1904 (2000).

[9] P. Xanthopoulos, W. A. Cooper, F. Jenko, Yu. Turkin, A. Runov J. Geiger, (to appear in *Phys. Plasmas*, 2009).

[10] S.P. Hirshman, W.I. van Rij, P. Merkel, *Comp. Phys. Commun.* **43** (1986).

[11] M.A. Beer, S.C. Cowley, G.W. Hammett, *Phys. Plasmas* **2**, 2687 (1995).

[12] G.H. Neilson, M.C. Zarnstorff, J.F. Lyon, the NCSX Team, *Journal of Plasma and Fusion Research* **78**, 214-219 (2002).

[13] J.N. Talmadge, V. Sakaguchi, F.S.B. Anderson, D.T. Anderson and A.F. Almagri, *Phys. Plasmas* **8**, 5165 (2001).

[14] G. Grieger, W. Lotz, P. Merkel, et al., *Phys. Fluids -B* **4**, 2081 (1992).

[15] G. Rewoldt, L.-P. Ku, and W. M. Tang. Phys. Plasmas 12, 102512 (2005).

[16] P. Xanthopoulos, F. Jenko, *Phys. Plasmas* **14**, 042501 (2007).

[17] J.N. Talmadge, (private communication).

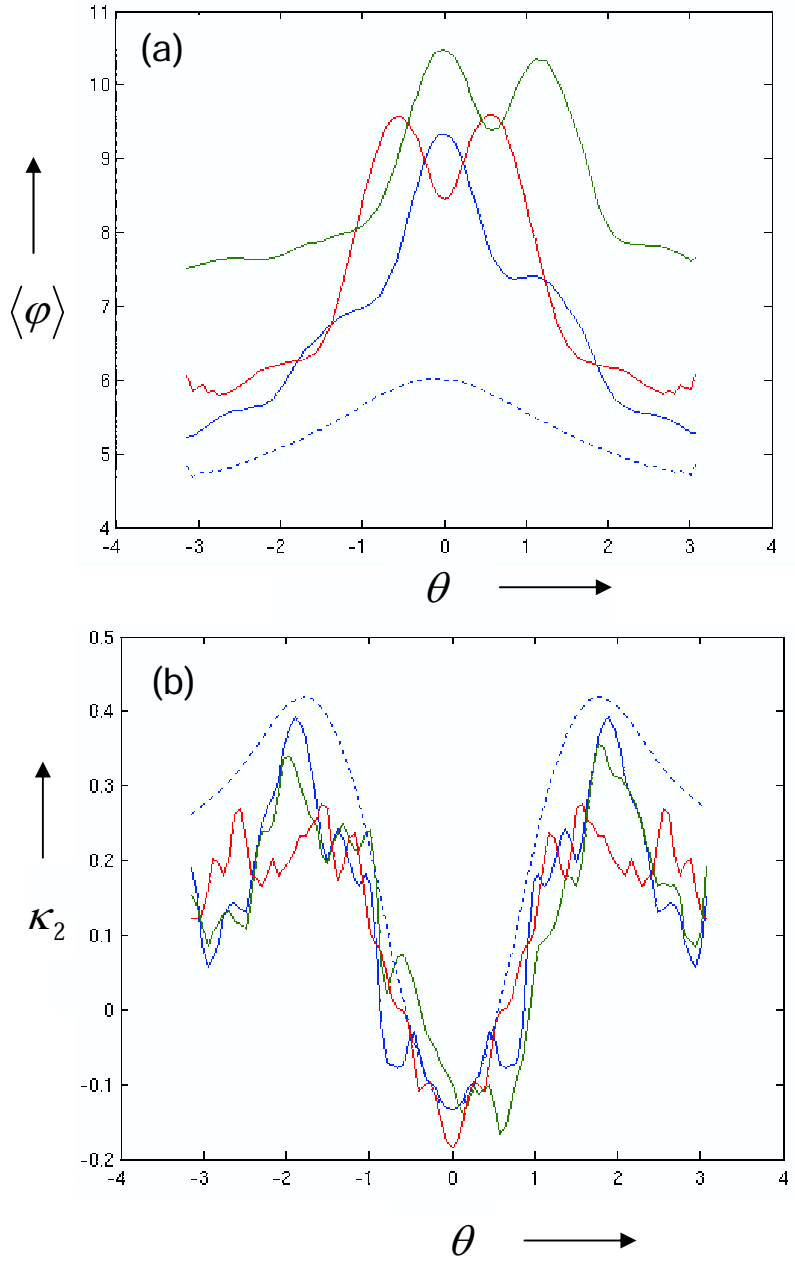

FIG. 1: (a)Averaged turbulent potential $\langle\phi\rangle(z = \theta)$ and (b)curvature $\mathcal{K}_2(z = \theta)$ for NCSX_sym (dashed), NCSX (solid).

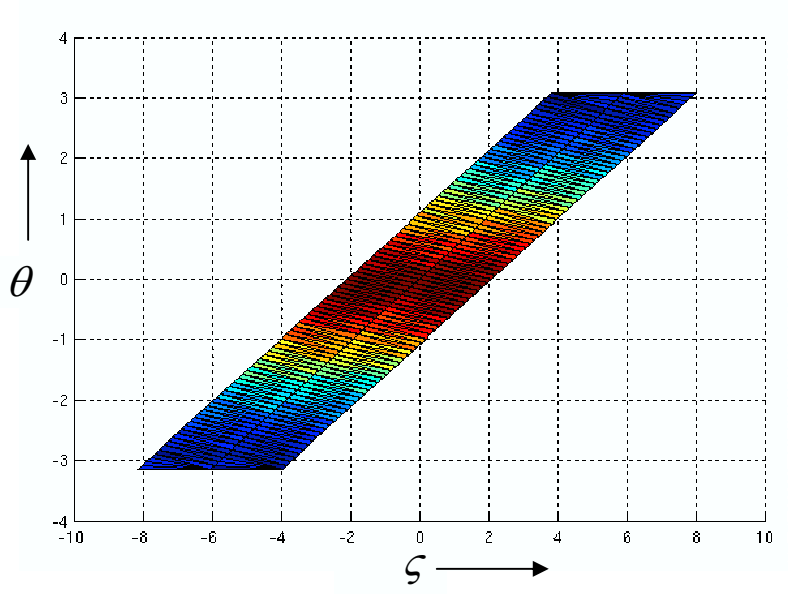

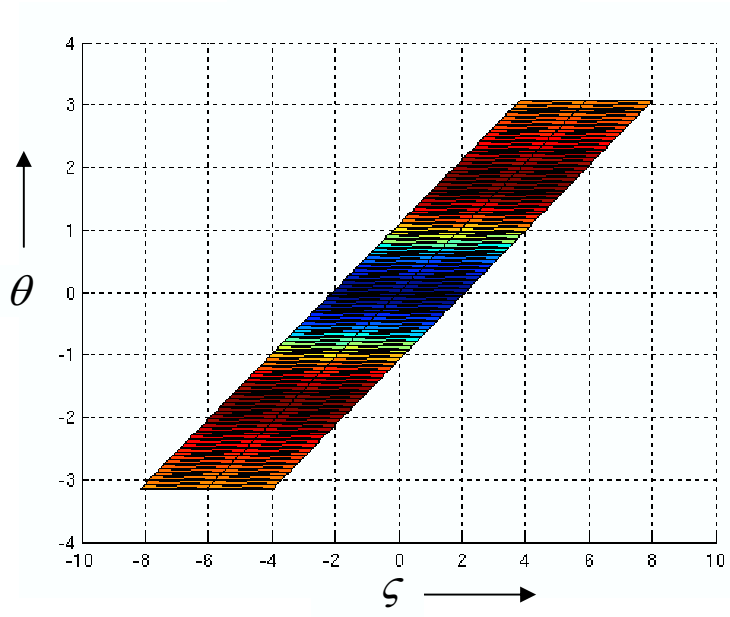

FIG. 2: (a)$\langle\phi\rangle(\theta,\zeta)$ and (b)$\mathcal{K}_2(\theta,\zeta)$ for NCSX_sym.

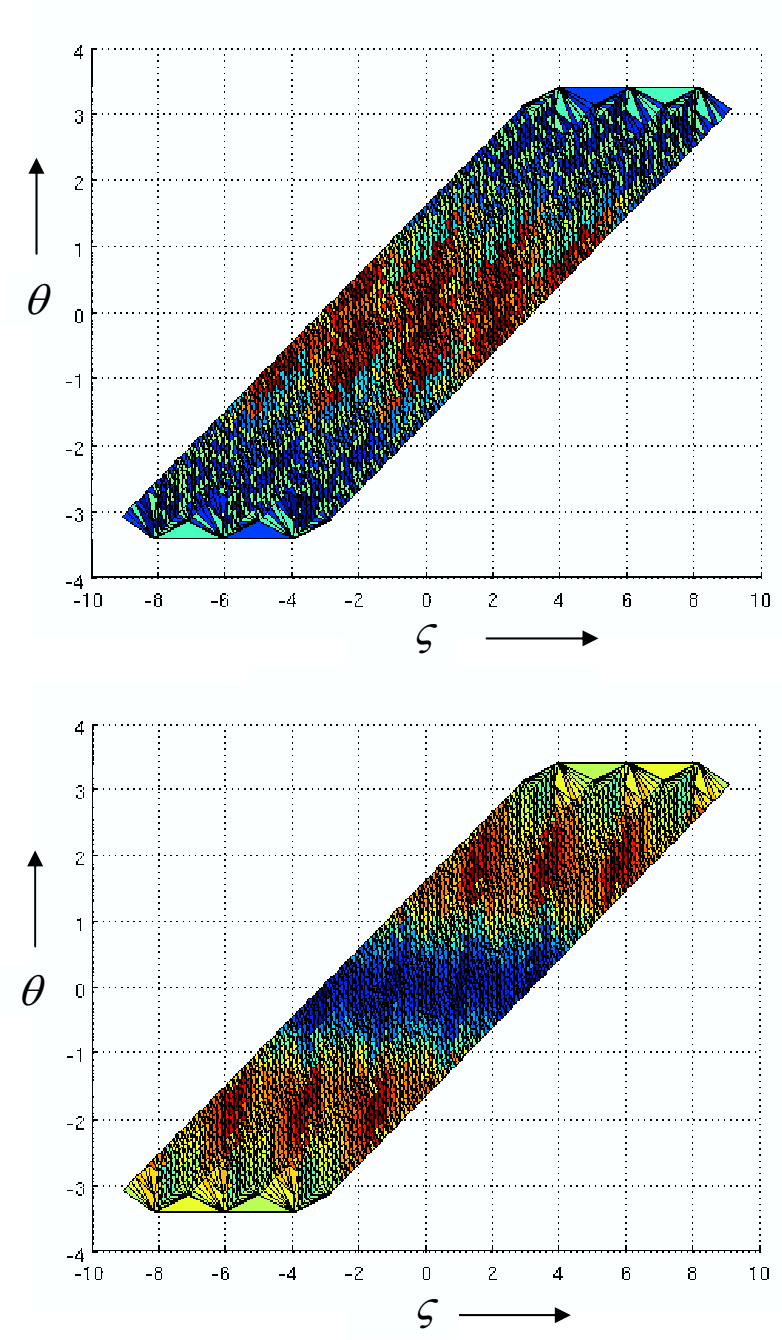

FIG. 3: (a)$\langle\phi\rangle(\theta,\zeta)$ and (b)$\mathcal{K}_2(\theta,\zeta)$ for NCSX.

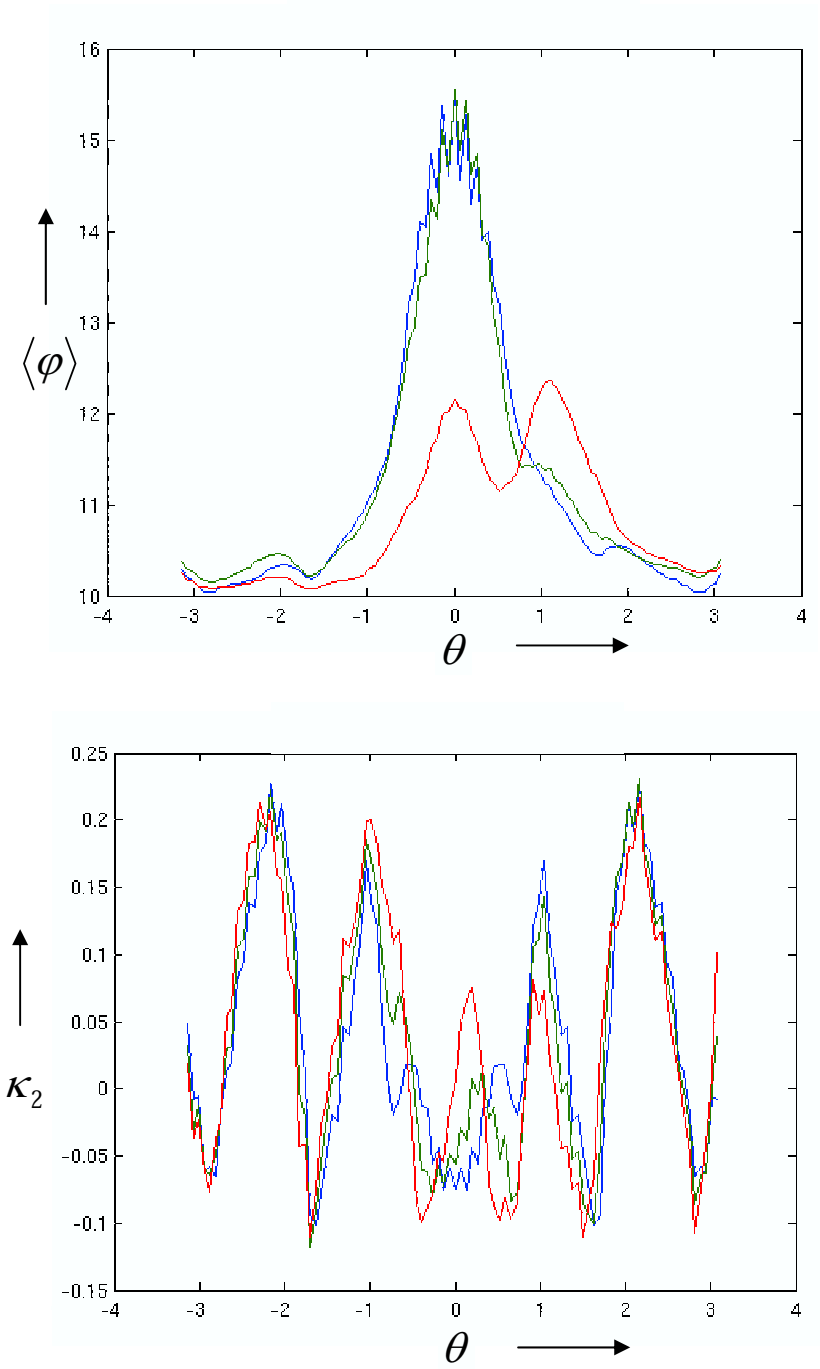

FIG. 4: (a)$\langle\phi\rangle(z=\theta)$ and (b)$\mathcal{K}_2(z=\theta)$ for W7X.

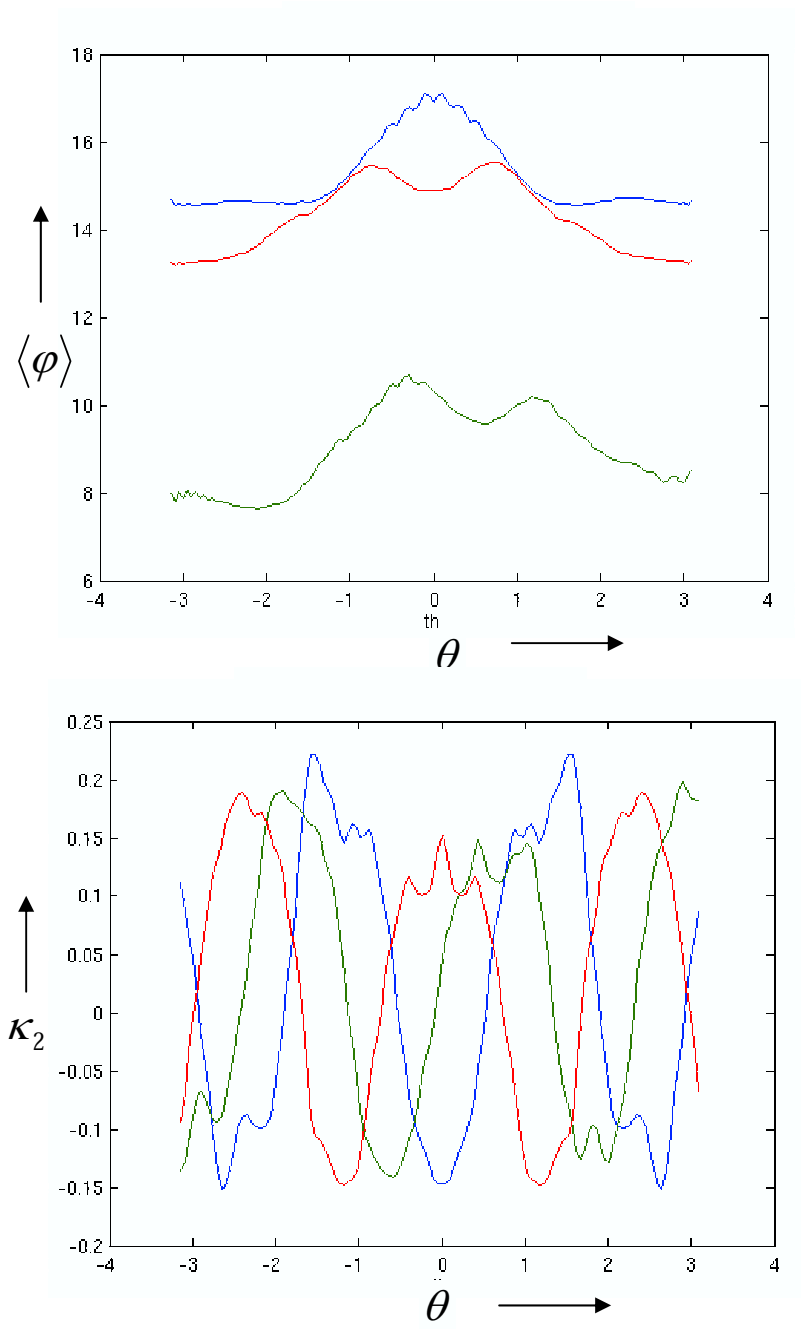

FIG. 5: (a)$\langle\phi\rangle(z=\theta)$ and (b)$\mathcal{K}_2(z=\theta)$ for HSX.

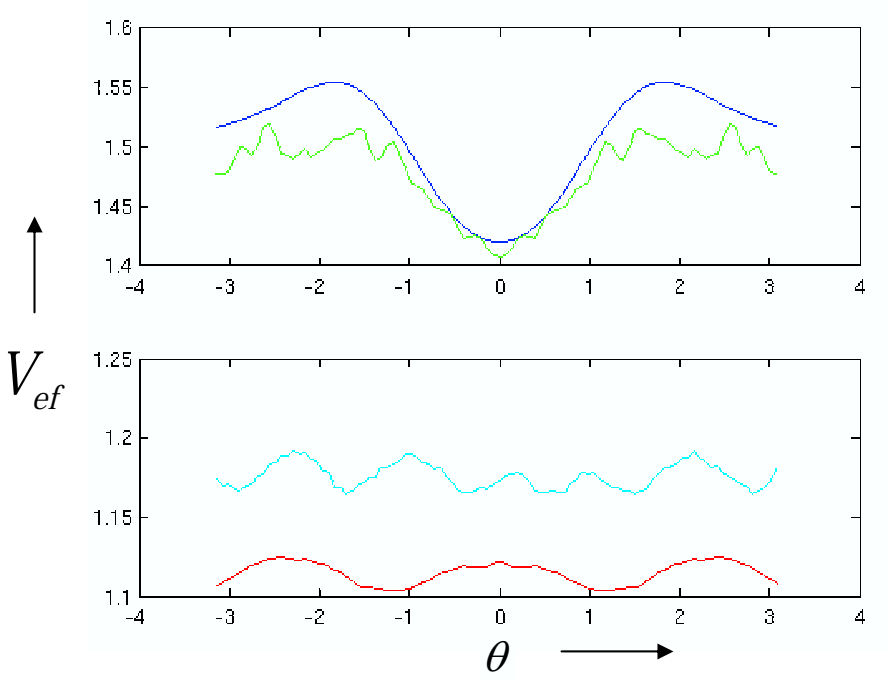

FIG. 6: Effective potential $V_{ef}(z = \theta)$ for tube $j = 2$ of NCSX_sym (blue), NCSX (green), HSX (red), and W7X (cyan).

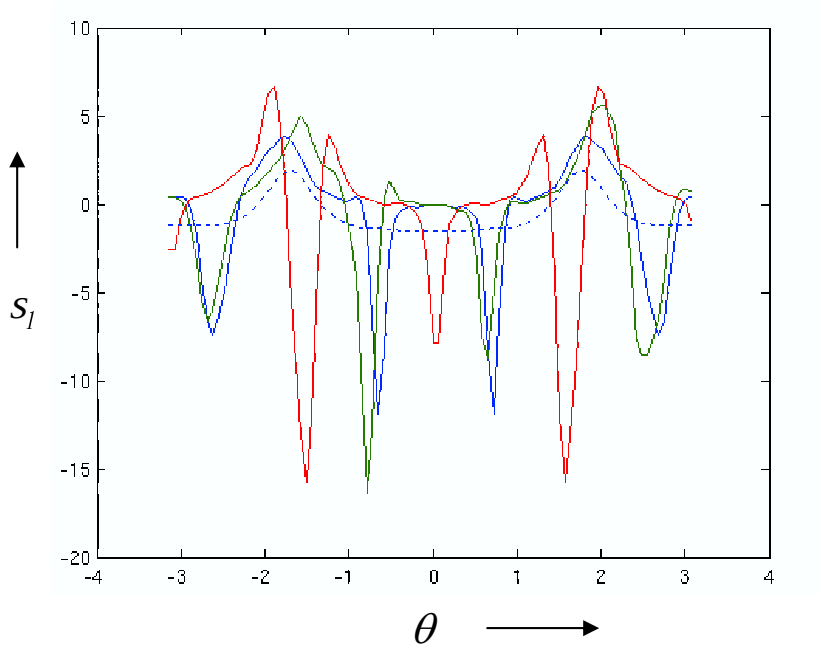

FIG. 7: Local shear $s_l(z = \theta)$ for NCSX_sym (dashed), NCSX (solid).

The Princeton Plasma Physics Laboratory is operated
by Princeton University under contract
with the U.S. Department of Energy.

Information Services
Princeton Plasma Physics Laboratory
P.O. Box 451
Princeton, NJ 08543

Phone: 609-243-2750
Fax: 609-243-2751
e-mail: pppl_info@pppl.gov
Internet Address: http://www.pppl.gov